Theoretical study of Schottky-barrier formation at epitaxial rare-earth-metal/semiconductor interfaces

Kris T. Delaney,[1] Nicola A. Spaldin,[2] and Chris G. Van de Walle[2]
[1]*Materials Research Laboratory, University of California, Santa Barbara, California 93106-5121, USA*
[2]*Materials Department, University of California, Santa Barbara, California 93106-5050, USA*
(Received 6 January 2010; revised manuscript received 29 March 2010; published 19 April 2010)

We present a detailed computational analysis of the atomic and electronic structure of ErAs/GaAs interfaces in polar and nonpolar crystallographic orientations. ErAs, a rocksalt semimetal, can be grown as a film with high-quality epitaxy on GaAs, a zinc-blende semiconductor. The As sublattice is continuous through the interface, providing a high-quality metal-semiconductor contact. We characterize the electronic structure of this interface using first-principles techniques based on density-functional theory. The Schottky barrier formed at the interface is highly sensitive to the interface orientation and the structural details. We deduce the primary mechanisms for Fermi-level pinning at specific energies within the band gap of the semiconductor.

DOI: 10.1103/PhysRevB.81.165312 PACS number(s): 73.20.−r, 73.40.Ns, 68.35.−p

I. INTRODUCTION

Interfaces between III-V and rare-earth-pnictide (RE-V) compounds have received much experimental and theoretical attention recently as a class of epitaxially matched metal-semiconductor contacts. Many rare-earth pnictides, especially arsenides and antimonides, are semimetallic and are stable in the rocksalt structure while III-Vs are semiconducting. As such, an interface between two of these materials can form a semimetal-semiconductor contact with an associated Schottky diode character. Due to most of their adopting, a rocksalt structure, the RE-Vs share a Bravais lattice with III-V zinc-blende semiconductors and have been shown to form epitaxially matched interfaces, for sufficiently thick films, with a continuous group-V sublattice if the lattice parameters of the two materials are matched closely.[1,2]

For decades, attempts have been made to explain the height of Schottky barriers by a number of different phenomenological models, such as the Mott-Schottky limit,[3] the Bardeen limit,[4] pinning of the Fermi level to so-called metal-induced gap (MIG) states,[5,6] and alignment of the Fermi level to the charge-neutrality level of the semiconductor.[7,8] However, there is still no single, robust model for *a priori* determination of the barrier height at metal/semiconductor interfaces. High-quality epitaxial interfaces such as those between RE-Vs and III-Vs provide an opportunity for rigorous studies of the formation of, and influences on, the barrier height without additional issues of structural disorder at the interface.

One of the most studied examples of RE-V/III-V interfaces is that between ErAs and GaAs. Owing to the close lattice match, it has been possible to grow, by molecular-beam epitaxy, coherent films of ErAs onto the pseudomorphically compatible GaAs substrate with a continuous As sublattice, provided more than four monolayers of ErAs are deposited. The modest lattice mismatch of 1.6% allows for coherent growth of ErAs films to thicknesses of many tens of angstroms. ErAs/GaAs planar interfaces have been studied both experimentally[1,2] and theoretically[9,10] since the initial discovery that the Schottky barrier height (SBH) depends sensitively on the crystallographic orientation of the interface[11] with a variation in barrier height of as much as 0.3 eV. Other types of electrical characterization have been performed, for instance, demonstrating the low noise of high-quality Schottky diodes.[12,13] Research is this area is driven by the desire to engineer the barrier height[14,15] for applications, including the creation of high-quality Ohmic contacts to III-V-based devices.[16]

In addition to planar interfaces, nanoparticles of ErAs have been successfully embedded into GaAs and InGaAs alloys with a continuous As sublattice. These nanostructured materials have interesting optical properties[17] and have been shown to exhibit strong phonon scattering resulting in enhanced thermoelectric properties.[18–20] Epitaxially embedded nanoparticles have also been proposed as a mechanism for improving tunneling in cascaded *pn* junctions as a route to more efficient solar cells,[21] and operate as fast recombination centers in terahertz photoconductive detectors.[22,23]

Understanding the origin of all of these properties requires a good description of the atomic and electronic structure of ErAs, as well as of interfaces between ErAs and GaAs. We have recently performed detailed investigations of the electronic structure of bulk ErAs,[24] including the effects of strain on the band structure.[25] In the present work, we focus on ErAs/GaAs interfaces. It has been demonstrated, both experimentally by varying alloy composition of the substrate,[11] and theoretically,[25] that the impact of strain on the electronic structure of ErAs is relatively minor. To quantify this, we use the volume deformation potential of the band overlap, for which we calculated a value of −4.49 eV.[25] This deformation potential leads to only a 0.05 eV correction to the band overlap for a 1% hydrostatic strain, and furthermore, any changes in the carrier density due to modification of the band overlap through strain are irrelevant to the electronic structure. Hence, much of the sensitivity of SBH to interface orientation is likely to arise from details of interfacial chemistry, stoichiometry, polarity, and the specific atomic structure.

The atomic structure of planar ErAs/GaAs interfaces has been experimentally characterized using scanning transmission electron microscopy (STEM),[2] demonstrating the stability of a polar termination of the semiconductor at (001) in-

 ©2010 The American Physical Society

terfaces, where the so-called "chain model" (explained below) is shown to be favored. However, fine details close to the interface, such as lattice spacing and the presence of low-density or disordered defects, are not completely resolvable due to limits of contrast and resolution.

In this paper, we explore the atomic and electronic structure of ErAs/GaAs planar interfaces, in polar and nonpolar crystallographic orientations, using first-principles computational methods. Theoretical studies were attempted previously[9,10] but considered only the (001) interface orientation.

II. COMPUTATIONAL APPROACH

A. Methodology

We employ first-principles calculations based on plane-wave density-functional theory (DFT) as implemented in the ABINIT (Refs. 26 and 27) software package.[28] Effects of electronic exchange and correlation are treated within the local-density approximation (LDA) with the Perdew-Wang[29] parameterization of Ceperley-Alder[30] electron-gas data. We treat the core-valence separation with the accurate projector-augmented wave (PAW) method,[31] which is especially efficient for large-Z elements and which, in principle, introduces no uncontrolled approximations beyond the frozen-core approximation. The PAW atomic data used here have been generated scalar relativistically by the authors using the ATOMPAW spherical-potential code.[32]

B. Treatment of Er *f* electrons

It is important to consider the approximations introduced in treating the Er $4f$ electrons. The treatment of these partially filled, strongly correlated states can affect the accuracy of fine quantitative details around the Fermi surface.[24] Our previous investigations[25] have shown that the correct qualitative description of the nonmagnetic electronic structure of the semimetal, including the features of the Fermi surface and a low free-carrier density, are obtained even within the LDA if the $4f$ electrons are included in the frozen-core partition of the PAW. The price of including the $4f$ states in the core partition is a small error in the free-carrier density[24] (7.6×10^{20} cm^{-3} versus the experimental value of 3.3×10^{20} cm^{-3}), which is also in part due to an error in the band overlap of the Kohn-Sham spectrum, as demonstrated by our *GW* calculations.[25]

The alternative choice, to include the $4f$ electrons in the valence, would introduce enormous quantitative and qualitative errors in the electronic structure[33] if the theoretical treatment used did not include the strong correlations required to split the Hubbard bands away from the Fermi level. A side effect of this type of error is a large erroneous hybridization of the Er $4f$ states with other states of the crystal while the correct electronic structure of ErAs includes $4f$ states that are essentially unmodified from those of an isolated Er^{3+} ion. With $4f$ states in the valence, an explicit treatment of the strong correlations fixes the erroneous hybridization.[24] Such an approach is feasible for the bulk solid but prohibitively expensive for the large supercells required for interface calculations. We therefore employ the frozen-core approximation for the Er $4f$ electrons to obtain a balance between a qualitatively correct electronic structure and computational complexity. We expect that this choice will not significantly affect any of our computed interface properties.

C. Numerical details

The Er PAW data is generated with a total valency of 11, with one $4f$ electron transferred to $5d$ resulting in the optimal configuration in the ErAs crystal. The core radius is 2.0 bohrs and the projectors are provided by pseudizing six partial waves. The As and Ga PAWs were generated with the $3d$ electrons in the core partition. For As, five partial waves are pseudized with a core radius of 2.2 bohrs while for Ga, four partial waves are pseudized with a core radius of 2.0 bohrs.

With the use of the PAW scheme, the plane-wave basis set for computing accurate properties is much reduced so that larger simulation cells can be accessed. The plane-wave energy cutoff required to converge the equilibrium lattice parameters to 0.1% and the total energy to within 0.1 mhartree/(f.u.) is only 18 hartree.

As for all metals with a sharp Fermi surface, ErAs requires careful convergence with respect to the Brillioun-zone sampling. Here, we use the efficient face-centered-cubic shifted-grid scheme with four $6\times6\times6$ Monkhorst-Pack grids.[34] The Fermi surface is smoothed with the second-order Methfessel-Paxton scheme[35] and a temperature of 0.1 eV to aid numerical convergence.

Using these PAW data sets and convergence parameters, we obtain bulk properties of ErAs and GaAs that are well matched with experiment. The lattice parameters are $a_0^{\mathrm{GaAs}}=5.58$ Å and $a_0^{\mathrm{ErAs}}=5.69$ Å, an underestimate of $\approx1\%$ compared with experiment, a typical error for the LDA. We have characterized the electronic structure of ErAs within our approach in earlier work.[25] Our GaAs band gap is 0.77 eV for the direct transition at Γ, compared with the zero-temperature experimental[36] gap of 1.52 eV. The indirect transitions from the valence-band maximum (VBM) at Γ to the conduction-band minima at L and X occur at 1.05 eV and 1.28 eV, respectively. These can be compared to zero-temperature experimental indirect gaps of 1.82 and 1.98 eV.[36]

D. Interface calculations

Investigations of interfaces from first principles are usually carried out using the supercell approach. Owing to the lack of an absolute reference for the potential of infinite crystals, the alignment of band structures at an interface cannot be determined using information about the constituent bulk materials alone. Rather, an explicit simulation of the interface must be undertaken, particularly in cases such as the present one in which details of interfacial structure are known to affect band alignments. Using periodic boundary conditions, a repeated heterostructure slab geometry is constructed. In order to isolate and study a single interface, a convergence study must be performed by inspecting the interface properties as the thickness of each slab is increased. For all results presented in Sec. III, we have rigorously con-

verged the results with respect to the slab thicknesses. For k-point sampling in interface supercell calculations, we use $6\times6\times1$ k points. A single k point suffices in the direction perpendicular to the interface, where the Brillouin zone collapses to zero thickness for infinitely large slabs.

E. Epitaxial strain

To determine the atomic structure of the interface, we relax all ionic and perpendicular lattice degrees of freedom to eliminate internal forces and perpendicular cell stresses. The length of the supercell is optimized using explicit minimization of the total energy. While this procedure is in practice subject to finite-basis errors in a plane-wave framework since the basis depends on the dimensions and shape of the unit cell, the errors can be essentially eliminated by increasing the plane-wave energy cutoff until the dimensions of the optimized cell are stable. In our calculations, the in-plane lattice constant is fixed to that of the DFT-LDA value of the semiconductor, simulating the experimentally relevant configuration in which the semiconductor provides a substrate for the biaxially strained ErAs film.[1] In common with usual DFT-LDA calculations, the lattice parameters of ErAs and GaAs are underestimated by approximately 1%, but, as detailed below, the error is similar for both materials so that the compressive *biaxial strain* applied to ErAs in our calculations closely matches that in experiment.

Since the ErAs layer is under biaxial strain, the slab relaxes out of plane by an amount that can be predicted by elastic theory given the elastic constants, which we have computed previously.[25] Under a homogeneous strain, the energy of the crystal can be written as

$$E = E_0 + \frac{1}{2}V\sum_{i=1}^{6}\sum_{j=1}^{6} C_{ij}e_ie_j + O[e^4], \tag{1}$$

where E is the total energy, V is the equilibrium volume of the unit cell, C_{ij} is the rank-4 elastic constant tensor (with three independent components for systems of cubic symmetry), and e_i is the linear Eulerian strain tensor. Both C_{ij} and e_i are written with tensor indices assigned according to the Voigt convention.

The linear Eulerian strain tensor for a homogeneous biaxial strain applied in the (001) plane is

$$e^{(001)} = \begin{pmatrix} \delta & 0 & 0 \\ 0 & \delta & 0 \\ 0 & 0 & \gamma \end{pmatrix}, \tag{2}$$

where δ is the strain applied in plane and γ is the resulting out-of-plane strain in equilibrium. Minimizing the total energy [Eq. (1)] of a system with cubic symmetry with respect to γ for fixed δ yields

$$\gamma = -2\frac{C_{12}}{C_{11}}\delta. \tag{3}$$

For ErAs, using our previously computed elastic constants,[25] $\gamma=-0.2055\delta$. The opposite sign of γ and δ implies that a compressive biaxial strain leads to expansion of the ErAs layers out of plane. Using a similar analysis for a strain δ' applied in the (011) plane,

$$\gamma' = -\frac{C_{11}+3C_{12}-2C_{44}}{C_{11}+C_{12}+2C_{44}}\delta'. \tag{4}$$

For ErAs, $\gamma'=-0.6588\delta'$. We compare these predictions to our fully relaxed DFT structures in Sec. III.

F. Determination of the Schottky barrier height

Once the ground-state atomic structure of our interface supercells has been deduced, we characterize the electronic structure. One of the most important features of a metal-semiconductor contact is the SBH. The barrier is an intrinsic property of the interface and is given simply by the relative alignment between the metal Fermi level and the semiconductor valence-band maximum (for the p-type barrier) or conduction-band minimum (for the n-type barrier) at the interface. While it is by now well known that the band structure obtained from Kohn-Sham theory cannot be associated with quasiparticle addition and removal energies,[37] the error in doing so tends to be systematic. The so-called band-gap problem of density-functional theory, which applies to semiconductors and insulators, is the best-known example of such an error, and within the LDA typically leads to an underestimation of the band gap of around 50%. However, it is often postulated that the majority of this error is attributed to the conduction band since an exact Kohn-Sham potential, if known, would yield the precise chemical potential (or energy of the valence-band maximum). While some counter examples to this postulate have been demonstrated, notably the Si/SiO_2 interface,[38] the common practice when using density-functional theory is to compute alignments between valence bands only. The analog of this practice for metal-insulator interfaces is the p-type SBH.

Band alignments (and SBHs) can be computed from first-principles supercell calculations using the macroscopic averaging method.[39] Our choice of reference is the electrostatic potential of the supercell, which contains all dipoles that may affect the alignment. The p-type SBH may be written as

$$\phi_p = \Delta\bar{V} + E_F - E_{\mathrm{VBM}}, \tag{5}$$

where $\Delta\bar{V}$ is the change in average electrostatic potential across the interface (positive if higher on the ErAs side), E_F is the metal Fermi level referenced to the average electrostatic potential of the metal and E_{VBM} is the valence-band maximum referenced to the average electrostatic potential of the semiconductor. $\Delta\bar{V}$ is obtained from an explicit simulation of the interface in a supercell calculation, and is sensitive only to the accuracy of the electron density, a rapidly converging quantity with respect to numerical details such as the size of the plane-wave basis and k-point sampling. E_F and E_{VBM} are bulk quantities, and can be obtained with great accuracy with respect to numerical details, such as the Brillouin-zone sampling, by simulating only the primitive rocksalt or zinc-blende unit cell. We note that the metal Fermi level can change when the lattice is biaxially strained. We have fully accounted for this effect by computing E_F for

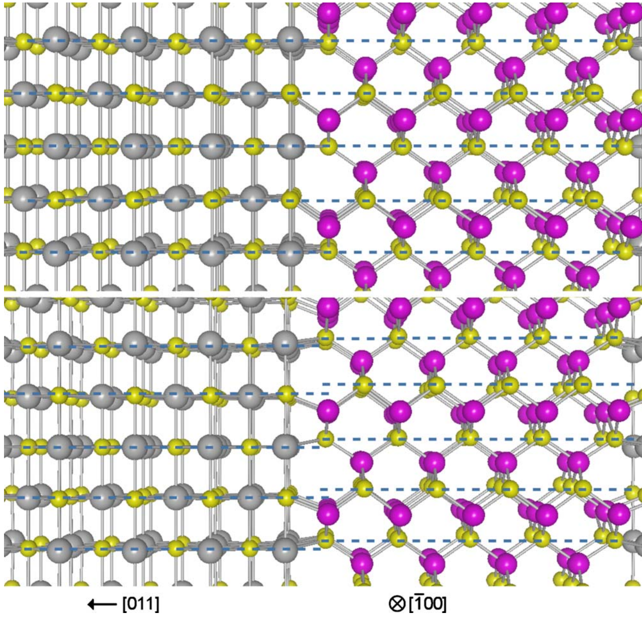

FIG. 1. (Color online) Relaxed (bottom) and unrelaxed (top) atomic structure of the (011) ErAs/GaAs interface, with ErAs to the left of the interface and GaAs to the right. The Er atoms are shown as large gray spheres, As small yellow spheres, and Ga medium red spheres. The horizontal dashed lines demark the As lattice planes, which are clearly displaced at the interface in accommodating the change in coordination.

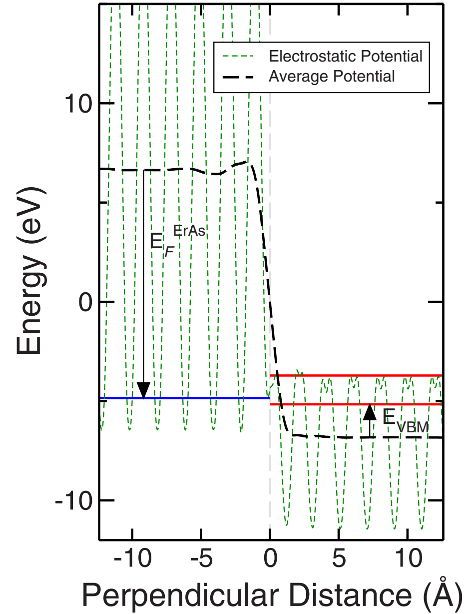

FIG. 2. (Color online) Planar averaged electrostatic potential (oscillating dashed green line) as a function of perpendicular distance from the (011) interface, defined to be zero at the first ErAs layer. Lattice-plane oscillations are evident, and are filtered with the macroscopic averaging technique (long-dashed black line). Referencing the ErAs Fermi level (blue line) and the GaAs valence-band maximum (lower red line) to the average potential yields the *p*-type SBH. The upper red line shows the conduction-band minimum of GaAs, corrected to the experimental band gap, assuming that the *p*-type SBH has no band-gap error. Note that the zero of energy is arbitrarily set to the average electrostatic potential of the entire supercell; what is important is the *difference* in potential across the interface.

a bulk ErAs unit cell with the same structure as the biaxially strained ErAs layer in the center of the relaxed slab that results from the interface calculation.

III. RESULTS AND DISCUSSION

A. GaAs/ErAs (011) interfaces

The (011) interface between rocksalt and zinc-blende structures is special because it provides a nonpolar termination for both structures. This property makes this interface orientation the most straightforward to treat computationally and converge the numerics rigorously. With the in-plane lattice constant determined by the optimized GaAs structure, 5.58 Å, ErAs is biaxially strained by −1.9%, close to the experimental strain value of −1.6%. From elastic theory [Eq. (3)], the out-of-plane strain for ErAs is expected to be +1.26%, leading to a layer spacing [$a/\sqrt{(2)}$ for (011) planes] of 4.08 Å. The explicitly relaxed DFT structure yields a layer spacing of 4.07 Å in excellent agreement with elastic theory.

The relaxed atomic structure is shown in Fig. 1. One clear feature emerges. The structure accommodates the change in cation coordination from fourfold to sixfold by slipping, parallel to the interface, the otherwise continuous As lattice planes by approximately 10% of the interplane spacing. Hence, the As sublattice is not perfectly continuous in the ground-state structure of the ideal, stoichiometrically balanced interface. While this distortion is not polar, and therefore does not significantly affect the SBH compared to the unrelaxed interface, it nevertheless provides an interesting and intrinsic structural feature of this interface orientation that may be experimentally resolvable.

The band alignment and SBH are shown in Fig. 2. In order to converge the band alignment to better than 0.01 eV, the supercell was constructed to contain nine layers of ErAs and nine layers of GaAs. We find $E_F=-11.50$ eV, $E_{\mathrm{VBM}}=1.66$ eV, and $\Delta\bar{V}=13.46$ eV. The final *p*-type SBH for the (011) interface orientation is 0.30 eV.

The barrier of $\phi_p^{011}=0.30$ eV corresponds approximately to a midgap alignment of the Fermi level, considering the underestimated Kohn-Sham band gap of GaAs (0.77 eV). It is especially interesting to try to understand the mechanism for the band alignment at such a perfect interface. Four different models are potentially relevant for a midgap alignment of the Fermi level: (1) the Mott-Schottky limit, which proposes that the SBH is equal to the work done by an electron in first escaping from the semiconductor into the vacuum and subsequently entering the metal. Hence, the *p*-type barrier is equal to the ionization potential of the semiconductor minus the work function of the metal. (2) Alignment of the Fermi level at the charge-neutrality level (CNL) of the semiconductor. (3) Pinning of the Fermi level to MIG states. (4) Pinning of the Fermi level to interface states (i.e., the Bardeen limit).

An understanding of the alignment mechanism is important in its own right, and would provide for better-justified

estimates of the possible corrections to the barrier height in the event that the GaAs band gap was corrected to the experimental value. Conventional wisdom states that the p-type barrier is less susceptible to band-gap errors, and hence only small corrections might be expected. Verification of this statement requires understanding the mechanism for the formation of the SBH.

Within the Mott-Schottky limit, we would expect a p-type SBH of 0.53 eV. We arrive at this figure from the *calculated* work function of ErAs (4.77 eV) and the Kohn-Sham ionization potential of GaAs (5.30 eV), both obtained by explicitly simulating a relaxed (011) surface and vacuum using the same numerical details as our interface calculations. This indicates that the Mott-Schottky limit is not valid for the nonpolar ErAs/GaAs interface. Furthermore, we have calculated the CNL of GaAs as the midvalue of energy between the k-point averaged valence band and the k-point averaged conduction band[40] (using the Baldereschi special point scheme[41]) and find the level to be 0.67 eV above the valence-band maximum. Hence, our calculations do not support pinning of the Fermi level at the semiconductor charge-neutrality level, either. We note that our particular way of calculating the CNL is not unique, and that more careful integrations over the Brillouin zone or inclusion of additional bands[42] will produce somewhat different values. But those observations also highlight that a model based purely on a lineup of the CNL will have limited predictive value (at least at the level of accuracy that we are aiming for).

Pinning to MIG states can be tested by probing the layer-by-layer species-projected density of states (DOS). The DOS is projected onto each site within the PAW augmentation sphere and summed over all angular momentum contributions. This local probe of the electronic structure, shown in Fig. 3, gives the electronic DOS projected into each atomic site and summed over all atomic sites within lattice planes parallel to the interface.

A finite density of electronic states is visible in the first layer of the semiconductor in the range of energies of the bulk band gap. In order to investigate the origin of these states further, we study the interface band structure shown in Fig. 4. We find that a number of states are occupied ($\varepsilon < \varepsilon_F$) with energies that are formally forbidden in the semiconductor. Hence, these states cannot correspond to bulk states in GaAs. Investigation of the probability amplitudes of two of these states (Fig. 5) confirms that they are interface states, in the sense that on the GaAs side their amplitude peaks at or near the interface, and then decays. Interface states at a semiconductor/semiconductor junction would be completely localized at the interface and decay on both sides. But in the case of a semiconductor/semimetal interface, where a continuous DOS is present in the energy region corresponding to the band gap of the semiconductor, these interface states necessarily correspond to extended states on the ErAs side, as is evident from Fig. 5. Still, we feel it is legitimate to regard these states as interface states since they can be correlated with bonding features across the interface that are also evident from inspection of the total electron charge density.

Contour plots of this density, in two different planes through the interface, are shown in Fig. 6. Both panels show that far from the interface, on the GaAs side, the bonding has clear covalent character and is highly directional; note the lobes in the charge density protruding from the As anion (the more electronegative atom) in the direction of the Ga atoms. On the ErAs side, far from the interface the bonding is ionic in nature and lacks directionality. But near the interface, the nature of the bonding changes. The top panel of Fig. 6 shows that the As atom in the outermost layer of ErAs acquires a certain amount of covalent character, and forms a directional

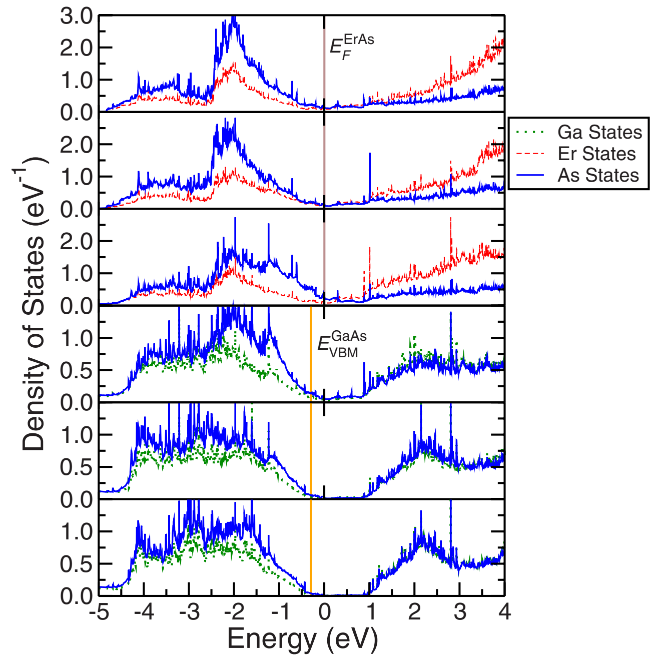

FIG. 3. (Color online) Layer-by-layer projected DOS for the (011) interface, drawn by species with Er (red dashed lines), Ga (green dotted lines), and As (blue solid lines). Panes in order from top to bottom: layers 3, 2, 1 of ErAs followed by layers 1, 2, 3 of GaAs. The values of E_F and E_{VBM} marked by vertical lines are obtained from accurate band-alignment procedures, not graphical details.

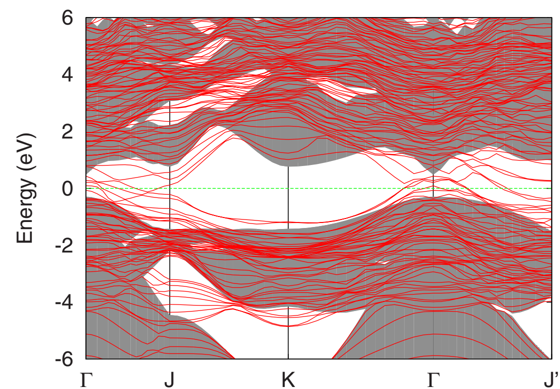

FIG. 4. (Color online) Supercell band structure of the ErAs/GaAs interface in the (011) orientation, aligned to zero at the Fermi energy. Shaded (gray) regions show the GaAs bulk band structure projected onto the two-dimensional Brillouin zone of the interface. Solid lines (red) show the band structure of the interface, which includes states in the band gap of the semiconductor.

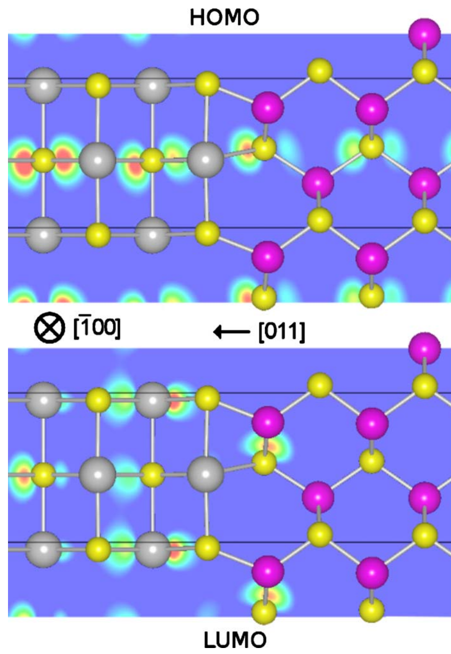

FIG. 5. (Color online) Sections of the probability amplitude of the highest occupied molecular orbital and lowest unoccupied molecular orbital states at Γ for the ErAs/GaAs (011) interface. ErAs states with significant weight are penetrating into the GaAs slab. The states are localized on As atoms, indicating strong directional bonding across the interface.

bond with the Ga atom across the interface. In fact, this tendency forms the driving force for the displacement of the As planes in ErAs with respect to the planes in GaAs, as discussed above. This inducement of covalent character in

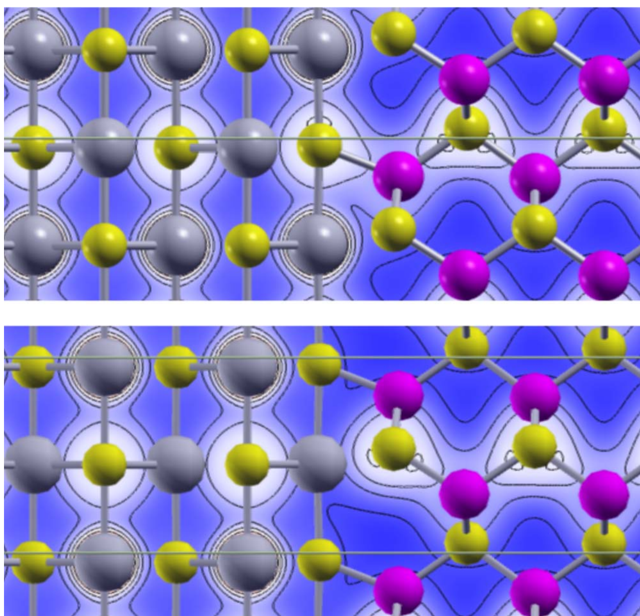

FIG. 6. (Color online) Contour plots of the total electron density in a cross section of the ErAs/GaAs (011) interface. Top panel: plane through the Ga atoms in the GaAs layer near the interface (also through the As atoms in the first ErAs layer). Bottom panel: plane through the As atoms in the GaAs layer near the interface.

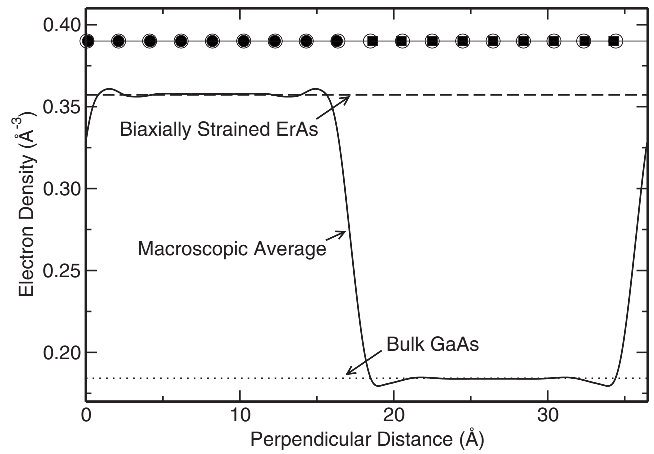

FIG. 7. Macroscopic average of the electron density throughout the supercell as a function of perpendicular distance from the interface, for a relaxed (011) interface. The electron density in the center of each slab matches the bulk electron densities well. The deviations near the interface are consistent with the change in bonding type across the interface, as discussed in the text. Symbols denote locations of lattice planes: filled circles for Er, open circles for As, and filled squares for Ga.

the As atom actually manifests itself also in the way this As atom bonds with the surrounding Er atoms. Notice, in particular, the development of directional (i.e., covalent) bonding between the As atom and the Er atom above it, within the last ErAs layer. This tendency to develop covalent bonding on the ErAs side also manifests itself in a local increase in the electron density, which is clearly seen in the macroscopic average of the electron density in the direction perpendicular to the interface, shown in Fig. 7.

The bottom panel of Fig. 6 shows that the As atom in the final GaAs has some directionality of bonding toward the interface; the tetrahedral sp^3 bonding configuration is imposed by its bonding to three surrounding Ga neighbors. But the bond across the interface cannot be a "good" covalent bond. An important reason for this is that there are not enough electrons available to form an additional two-electron bond. Indeed, as pointed out above, within the ErAs slab, each layer is electrically neutral and no additional electrons can be provided by the ErAs to form covalent bonds across the interface. On the GaAs side, the last layer is terminated with Ga and As dangling bonds (DBs), with a total of two electrons per two-atom surface cell. This situation is exactly the same as on the nonpolar (011) surface but there the energetically favorable solution is for the Ga-As dimers to tilt, and for the As DB to be filled with two electrons and the Ga DB to remain empty. At the GaAs/ErAs interface, however, there would be an opportunity to form a Ga-As bond *and* an As-Er bond (or As DB), as described above; and two electrons are clearly insufficient for that purpose.

Having arrived at this understanding of the nature of the bonding and its effects on the electronic structure, we return to the issue of identifying the mechanism that drives alignment of the Fermi level. One could argue that the interface states discussed above fit within the MIG states model since they correspond to metal-induced states that decay some dis-

tance into the semiconductor. While this is generically true, this view does not take advantage of the insights into the microscopic features of the states and their origins. Furthermore, the generic MIG states model would not predict at which energy the Fermi level would be pinned (beyond an estimate based on the position of the CNL, which was already discussed above).

The fact that the interface states, and their connection to specific atomistic features, play a key role in the Fermi-level alignment seems to fit most closely with the Bardeen model for metal/semiconductor interfaces. As discussed above, both Ga-As and Er-As bonds would, in principle, form across the interface but an insufficient number of electrons is available to allow formation of two covalent bonds. Strong covalent bonds would give rise to states with energies well below the GaAs VBM; the weaker bonds across the interface (akin to DBs) give rise to states with energies within the GaAs band gap. These states are filled with electrons, starting at energies near the VBM, until the system is charge neutral. Since this process is also coupled to details of structural distortions, it would be very hard to *a priori* predict where the Fermi level will end up, based on simple notions such as CNLs or energies of Ga and As DBs. Our best guess would be that the Fermi level would be pinned somewhere between the As DB level and the Ga DB level (but probably not exactly midway between those two, as would be the case in a CNL-lineup model).

These insights do give us a means, however, of assessing how corrections to the LDA band gap may affect the SBH. Calculations for CNLs as well as for Ga and As DBs (Ref. 43) have indicated that band-gap corrections (e.g., based on hybrid functionals) give rise to an upward shift of these levels by ≈ 0.35 eV. Applying this correction to the LDA result for the *p*-type SBH for the (011) interface, we would find a corrected value of $0.30+0.35=0.65$ eV, within 0.05 eV of the experimental value.[11]

B. GaAs/ErAs (001) interfaces

The (001) interface orientation implies nonpolar rocksalt and polar zinc-blende terminations. Experimentally, interfaces are usually formed in this orientation due to the availability of high-quality substrates. It is hence a particularly important case for which to understand the electronic and atomic structures.

The polar nature of the semiconductor results in two possible ideal, unreconstructed interfaces with a continuous anion sublattice:[9] Ga-terminated (the "chain" structure) and As-terminated (the "shadow" structure). Note that these interfaces are not stoichiometrically balanced, and include an excess of cations (anions) for the chain (shadow) structure. In order to avoid long-range fields being set up in our simulation cell, we terminate with equal polarity on both sides of the GaAs slab.[44]

The layer strain expected from Eq. (4) is 0.39% for both chain and shadow structures. This leads to an expected layer spacing of 5.71 Å. The calculated layer spacings in the relaxed structures for both chain and shadow terminations are 5.71 Å, again in excellent agreement with elastic theory.

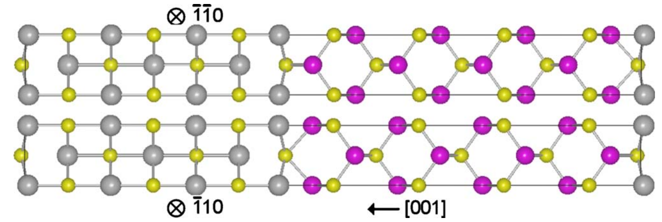

FIG. 8. (Color online) Relaxed atomic structure of the (001) ErAs/GaAs interface in the Ga-terminated chain structure. The Er atoms are shown as large gray spheres, As small yellow spheres, and Ga medium red spheres. Buckling of the terminating ErAs layer is evident, which yields dipoles at the interface that modify the band alignment by more than 1 eV.

We first investigate the chain structure, which is experimentally observed to be the most stable using STEM imaging.[2] The relaxed chain structure is shown in Fig. 8. It is clear that the polar termination of the semiconductor leads to buckling of the lattice planes, with relaxations well localized in the interfacial region. Such bucklings induce dipoles at the interface and are thus extremely important for determining the electronic structure. Inclusion of these relaxations lowers the SBH by more than an electron volt.

The presence of this buckling, combined with the polar nature of the semiconductor slab, renders obtaining converged properties much more difficult than in the case of the nonpolar (011) interface orientation. Indeed, significant errors are induced if the number of layers in each slab of the heterostructure is too small. We find a minimum of 11 ErAs and 9 GaAs layers are required to recover the bulk atomic structure, to within 5 mÅ in the ErAs layer spacing, in the center of each slab and to converge the Schottky barrier height to within 0.05 eV. In the center of the ErAs slab, the As planes parallel to the interface are spaced in accordance with the predictions from elastic theory. At the interface, however, an extra 0.2–0.4 Å lattice-plane spacing is observed (Fig. 9). This spacing arises from the ideal structure containing very short next-nearest-neighbor cation (Er-Ga) distances. As a result, there is a strain on the unit cell perpendicular to the interface which, when allowed to relax, leads to an increased spacing in the interface region. Further quantification shows that the Er-Ga distance across the interface is increased from the ideal value of 2.5–2.9 Å. This distance is in excellent agreement with structural characterization from STEM images,[2] where it was found to be 2.9 ± 0.2 Å, and with previous theoretical studies.[10]

In order to demonstrate that the changes in layer spacing are confined to the interface, and that the supercell is large enough to recover the bulklike structure of the ErAs and GaAs slabs in the center, we have plotted the interlayer spacing as a function of the perpendicular distance from the interface in Fig. 9. It can be clearly seen that bulklike regions are recovered in the center of each slab.

With the relaxed atomic structure, we obtain a *p*-type SBH of $\phi_p^{(001)c}=1.26$ eV. For the Kohn-Sham band structure of GaAs, which has a minimum band gap at Γ of 0.77 eV, it appears that the Fermi level of the metal is actually higher in energy than the conduction-band minimum of the semiconductor. Such an alignment would result in charge flow from

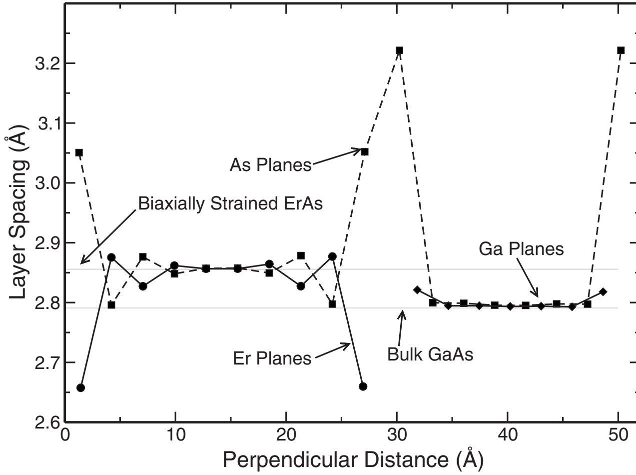

FIG. 9. Interlayer spacing as a function of perpendicular distance from the interface for a relaxed (001) interface in the chain structure. It is evident that the structure recovers a bulklike region in the center of each slab, despite the large buckling of layers present at the interface.

the metal to the semiconductor, thus rendering the calculations unreliable due to the Kohn-Sham band-gap error. However, upon careful inspection, we find no evidence of such a charge flow (see Fig. 10). The solution to this apparent dichotomy is partially provided by inspecting the set of Brillouin-zone sample points used in the interface calculation. The k mesh does not include the Γ point, which would sample the minimum band gap. Owing to the large dispersion (low effective mass) of the conduction band of GaAs, sampling even a little away from Γ significantly increases the band gap. Additionally, the GaAs slab in our calculations has a finite thickness which introduces small band-edge shifts due to quantum confinement. The combined effect of k-point sampling and quantum confinement in the slab is to shift the effective conduction-band minimum to higher energy and the

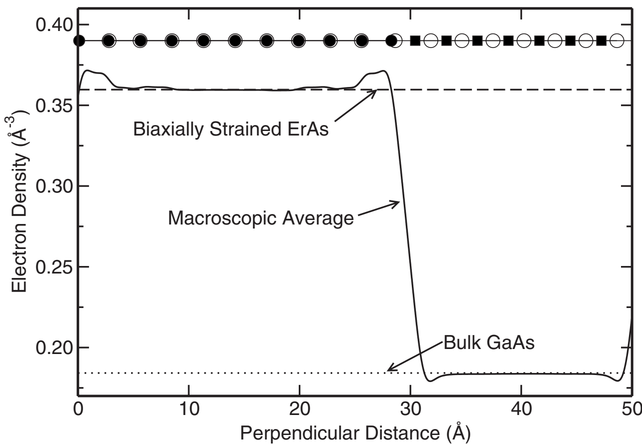

FIG. 10. Macroscopic average of the electron density throughout the supercell as a function of perpendicular distance from the interface, for a relaxed (001) interface in the chain structure. The electron density in the center of each slab matches the bulk electron densities well. Symbols denote locations of lattice planes: filled circles for Er, open circles for As, and filled squares for Ga.

valence-band maximum to lower energy. Any interface states, however, are relatively dispersionless and are localized at the interface. Hence, they are not strongly affected by such issues. The result, after accounting for the effects of quantum confinement and k-point sampling is that the metal Fermi level is actually aligned close to, but below, the effective conduction-band minimum of the slab.

It is once again useful to consider the type of mechanism that drives the band lineup, in this case leading to alignment of the metal Fermi level with the semiconductor conduction-band minimum. The most obvious candidate for the alignment mechanism is related to the interface states that exist at polar interfaces. Assuming that the tetrahedral (sp^3) coordination of GaAs is maintained right up to the interface, we find that Ga DBs are present in the chain structure. Due to the lack of stoichiometric balance, these DBs are partially filled. Each (001) layer of ErAs is charge neutral; therefore, for the purposes of electron counting, the termination of the chain structure is equivalent to the case of an unreconstructed Ga-terminated GaAs (001) surface, in which the surface Ga atoms each have two DBs, each occupied with 3/4 electrons, i.e., a total of 1.5 electrons per Ga atom.

Cation DBs typically have energies close to the conduction band of the semiconductor. Occupying them with electrons is energetically costly. It would therefore be energetically favorable if these electrons could be transferred out of the DBs and into the semimetal. However, as already noted above, no evidence of such electron transfer is found. Indeed, if electrons were transferred into the semimetal, the Fermi level in the semimetal would need to move in order to accommodate this extra charge. Note that, unlike in a doped semiconductor, where charge in depletion layers is *fixed* charge, the extra charge in a semimetal occurs in the form of free carriers. These carriers efficiently screen the electric fields that would be created due to charge transfer. The net result is that the Fermi level of the semimetal becomes pinned at the level that gives rise to a charge-neutral interface (with 1.5 electrons per Ga atom in the Ga-dangling-bond-induced interface state). This model is confirmed by inspecting the layer-by-layer projected density of states (Fig. 11), which clearly resolves the DB.

For the shadow termination, the situation is the exact analog of the chain termination with DBs formed from As sp^3 states. These states are close to the valence band so that the Fermi level is pinned near the valence-band maximum. Hence, $\phi_p^{(001)s}=0.00$ eV. The relaxed shadow structure and layer-by-layer DOS are shown in Figs. 12 and 13, respectively.

C. Reconstructions at (001) interfaces

The ideal relaxed (001) interface structures are predicted by DFT to form nonrectifying contacts, with the Fermi level having no barrier to the conduction band for the chain structure and no barrier to the valence band for the shadow structure. Based on the physical understanding of the bonding at these interfaces, discussed above, we expect that band-gap corrections would not qualitatively change these alignments. Such a barrier-free contact contradicts the results of

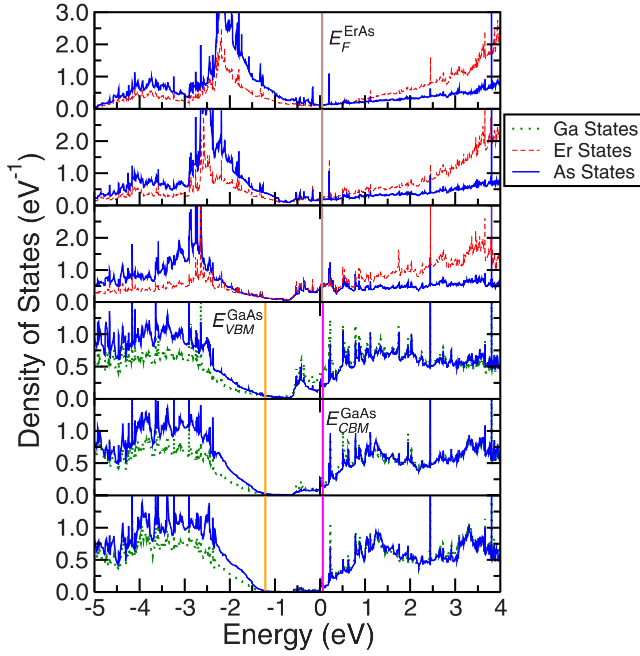

FIG. 11. (Color online) Layer-by-layer projected DOS for the (001) chain-structure interface with Er in red dashed lines, Ga in green dotted lines and As in blue solid lines. Panels in order from top to bottom: layers 3, 2, 1 of ErAs followed by layers 1, 2, 3 of GaAs. Values of E_F, E_{VBM}, and E_{CBM} as obtained from band-alignment procedures are marked by vertical lines. E_{CBM} is obtained for the k points that are sampled in the GaAs slab. An interface state is clearly visible in the upper part of the semiconductor band gap. This state is partially filled and the Fermi level is pinned within the energy range of this state.

experimental measurements, where a finite SBH ($E_F \sim 0.4-0.5$ eV above the valence-band maximum) is found for the (001) interface.[11] The interfaces investigated so far are unreconstructed, i.e., they maintain the 1×1 periodicity of the bulk. Here, we investigate interfacial reconstructions by allowing for larger interfacial unit cells. In the spirit of the electron counting rule, the motivation is to decrease the number of occupied Ga DBs and/or the number of unfilled As DBs.

We evaluate which interface configuration is the most stable, from a set of candidates with varying degrees of complexity, by calculating the formation energy of the interface. In all cases, we begin with the chain structure and increase

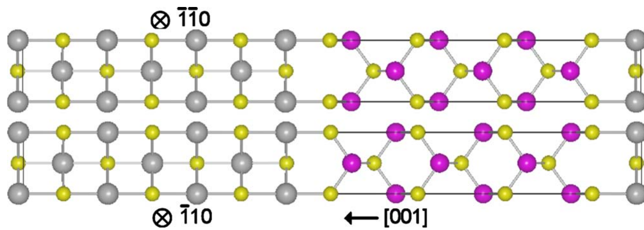

FIG. 12. (Color online) Relaxed atomic structure of the (001) ErAs/GaAs interface in the As-terminated shadow structure. Er atoms are shown as large gray spheres, As small yellow spheres, and Ga medium red spheres.

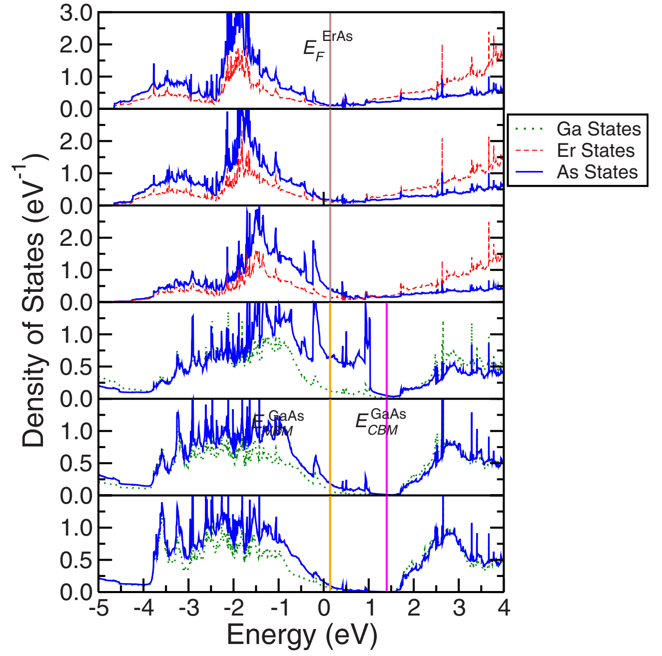

FIG. 13. (Color online) Layer-by-layer projected DOS for the (001) shadow-structure interface with Er in red dashed lines, Ga in green dotted lines, and As in blue solid lines. Panels in order from top to bottom: layers 3, 2, 1 of ErAs followed by layers 1, 2, 3 of GaAs. Values of E_F, E_{VBM}, and E_{CBM} as obtained from band-alignment procedures are marked by vertical lines. An interface state is clearly visible in the lower part of the semiconductor band gap.

the in-plane unit cell by a factor of 2, 4, or 8 in area. These correspond to (2×1), (2×2), and (2×4) interface unit cells, respectively. We then introduce Ga vacancies to restore stoichiometry and relax the cells.

The formation energy of an interface in our supercells can be calculated using total energies,

$$E_{\mathrm{form}} = \frac{1}{2}(E_{\mathrm{tot}}^{sc} - N_{\mathrm{ErAs}}E_{\mathrm{tot}}^{\mathrm{ErAs}} - N_{\mathrm{GaAs}}E_{\mathrm{tot}}^{\mathrm{GaAs}} - N_{\mathrm{Ga}}\mu_{\mathrm{Ga}} - N_{\mathrm{As}}\mu_{\mathrm{As}} - N_{\mathrm{Er}}\mu_{\mathrm{Er}}), \quad (6)$$

where E_{form} is the formation energy of a single interface. We subsequently normalize the formation energy, in the case of larger in-plane unit cells, for comparison with (1×1) interfaces. Equation (6) is valid in the case that both interfaces in the supercell are equivalent, which is always the case for our simulations. E_{tot}^{sc} is the DFT total energy of the supercell calculation containing both interfaces, N_{ErAs} and N_{GaAs} are the number of formula units of ErAs and GaAs contained in the supercell, and $E_{\mathrm{tot}}^{\mathrm{ErAs}}$ and $E_{\mathrm{tot}}^{\mathrm{GaAs}}$ are the total energies of primitive unit cells of bulk ErAs and GaAs. The remaining terms are required for nonstoichiometric situations in which the supercell does not contain a whole number of formula units of either ErAs or GaAs. In particular, the chain and shadow terminations of the (001) interface always contain a single additional or deficient Ga per (1×1) interface cell compared with N_{GaAs}, such that $N_{\mathrm{Ga}} = \pm1$. Finally, μ_{Ga} is the gallium chemical potential, which is a variable in our calcu-

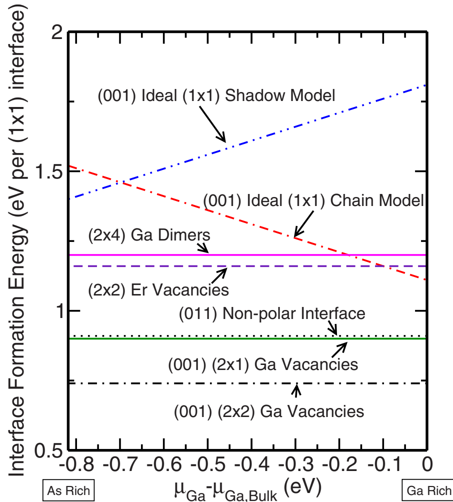

FIG. 14. (Color online) Interface formation energy per (1×1) interface unit cell. Different candidate structures are evaluated for the (001) polar ErAs/GaAs interface. Formation energies of nonstoichiometric supercells depend on the Ga chemical potential.

lations (corresponding to the experimental notion that growth can proceed under Ga-rich or Ga-poor conditions, or anything in between). The chemical potential is referenced to the energy of a bulk gallium phase, and is bounded by $\mu_{\mathrm{Ga}}=0$ in the gallium-rich limit and by $\mu_{\mathrm{Ga}}=\Delta H_f^{\mathrm{GaAs}}$, the formation enthalpy of GaAs, in the arsenic-rich limit. Only interfaces with unequal numbers of anions and cations (Er and Ga are both trivalent) have any dependence on the chemical potential.

In order to expedite the search, we initially evaluated the interface formation energy based on supercells with only three ErAs and three GaAs layers. These supercells are not large enough to accurately evaluate SBHs but the formation-energy *differences* are accurate enough to provide information about relative stability. For selected interfaces [chain and shadow (1×1) (001) and the (001) interface structure with the lowest formation energy], systematically growing the slabs up to 11 layers shows a variation in formation energy on the order of 0.1 eV. The interface formation energies are plotted as a function of the gallium chemical potential in Fig. 14. Only the (1×1) chain and shadow (001) interfaces have any dependence on the chemical potential because other interfacial structures are chosen to have an equal number of anions and cations. For the reconstructed (2×2) interfaces, the missing atoms were arranged in a "checkerboard" pattern. Our calculations predict that a (2×2) structure containing two gallium vacancies per unit cell is the most stable for any value of the gallium chemical potential. The ideal unreconstructed chain and shadow structures are higher in energy for all chemical potential values. The stability of the (2×2) structure is not surprising when considering elementary electron counting. The structure has two gallium atoms per interface cell, each with two DBs. These provide a total of three electrons. The four underbonded As atoms each have a single dangling bond and 1.25 electrons. In total, there are eight electrons in the interface region, which can completely fill the four As DBs. The Ga DBs end up being empty, and hence the electron counting rule is satisfied.

We note that for GaAs surfaces, a (2×4) structure with rows of dimers would be the most stable structure. Our calculations allow for such a possibility but we find this arrangement to be unfavorable for interfaces.

For the interface structure that emerges as having the lowest formation energy, we now increase the size of the supercell to seven ErAs and seven GaAs layers. The resulting p-type SBH is $\phi_p=0.08$ eV, i.e., the Fermi level is quite close to the valence-band maximum. This result is in better agreement with experiment ($E_F\sim0.4$–0.5 eV above the valence-band maximum[11]) than the values we obtained for unreconstructed interfaces but still off by more than 0.3 eV. Intriguingly, the same upward shift by 0.35 eV (associated with band-gap corrections beyond LDA) that we discussed in the context of (011) interfaces would bring the present results for the (001) interface in close agreement with experiment. We also note that, while the bare LDA results for SBHs are not in agreement with experimental results, they follow the experimentally observed trend, namely, a decrease of ≈0.2 eV in ϕ_p in changing from the (011) to the (001) interface orientation.

IV. CONCLUSIONS

In conclusion, we have performed extensive and numerically accurate studies of the atomic and electronic structure of ErAs/GaAs interfaces in polar (001) and nonpolar (011) orientations. Our DFT-LDA calculations recover known features of the interface geometry while predicting new features such as the anion lattice-plane displacement in the (011) interface and the lowering of interfacial energy by reconstructions at the (001) interface. Our calculations demonstrate a Schottky-barrier lineup at approximately midgap for the (011) interface orientation while our calculations for (001) polar interfaces show pinning of the Fermi level at dangling-bond states and an Ohmic contact for ideal unreconstructed structures. Among our trial reconstructed interfaces, we found a 2×2 structure that is stoichiometrically balanced to be energetically favored. This structure displays rectifying character, in agreement with experiment. While our numerical values of the SBHs are lower than the experimental ones by 0.3–0.4 eV, presumably a manifestation of the Kohn-Sham band-gap problem, we do recover the trend that the p-type SBH differs by 0.2 eV between the (011) and (001) interface orientations. We attribute the Fermi-level lineup to the tendency for covalent bonding across the interface for all orientations, an example of the Bardeen limit of Schottky barrier models, and note that the change in bonding character with interface orientation explains the observed sensitivity of barrier heights to this orientation.

ACKNOWLEDGMENTS

We are grateful for fruitful discussions with A. Gossard, C. Palmstrøm, S. Stemmer, J. LeBeau, J. D. Zimmerman, and J. Weber. This work was supported by the MRSEC

Program of the National Science Foundation under Award No. DMR05-20415 and also made use of computing facilities at the San Diego Supercomputer Center (TeraGrid) and at the California Nanosystems Institute (NSF under Grant No. CHE-0321368). Crystal structure images were generated with VESTA (Ref. 45).

---

[1] C. J. Palmstrøm, N. Tabatabaie, and S. J. Allen, Jr., Appl. Phys. Lett. **53**, 2608 (1988).
[2] D. O. Klenov, J. M. Zide, J. D. Zimmerman, A. C. Gossard, and S. Stemmer, Appl. Phys. Lett. **86**, 241901 (2005).
[3] N. F. Mott, Proc. Cambridge Philos. Soc. **34**, 568 (1938).
[4] J. Bardeen, Phys. Rev. **71**, 717 (1947).
[5] V. Heine, Phys. Rev. **138**, A1689 (1965).
[6] W. Mönch, Rep. Prog. Phys. **53**, 221 (1990).
[7] C. Tejedor, F. Flores, and E. Louis, J. Phys. C **10**, 2163 (1977).
[8] J. Tersoff, Phys. Rev. Lett. **52**, 465 (1984).
[9] E. Tarnow, J. Appl. Phys. **77**, 6317 (1995).
[10] W. R. L. Lambrecht, A. G. Petukhov, and B. T. Hemmelman, Solid State Commun. **108**, 361 (1998).
[11] C. J. Palmstrøm, T. L. Cheeks, H. L. Gilchrist, J. G. Zhu, C. B. Carter, B. J. Wilkens, and R. Martin, J. Vac. Sci. Technol. A **10**, 1946 (1992).
[12] A. Young, J. Zimmerman, E. Brown, and A. Gossard, Appl. Phys. Lett. **88**, 073518 (2006).
[13] A. C. Young, J. D. Zimmerman, E. R. Brown, and A. C. Gossard, J. Appl. Phys. **101**, 084509 (2007).
[14] J. D. Zimmerman, E. R. Brown, and A. C. Gossard, J. Vac. Sci. Technol. B **23**, 1929 (2005).
[15] J. D. Zimmerman, A. C. Gossard, A. C. Young, M. P. Miller, and E. R. Brown, J. Vac. Sci. Technol. B **24**, 1483 (2006).
[16] U. Singisetti, J. D. Zimmerman, M. A. Wistey, J. Cagnon, B. J. Thibeault, M. J. W. Rodwell, A. C. Gossard, S. Stemmer, and S. R. Bank, Appl. Phys. Lett. **94**, 083505 (2009).
[17] M. Scarpulla, J. Zide, J. LeBeau, C. Van de Walle, A. Gossard, and K. Delaney, Appl. Phys. Lett. **92**, 173116 (2008).
[18] W. Kim, J. Zide, A. Gossard, D. Klenov, S. Stemmer, A. Shakouri, and A. Majumdar, Phys. Rev. Lett. **96**, 045901 (2006).
[19] J. M. O. Zide, D. Vashaee, Z. X. Bian, G. Zeng, J. E. Bowers, A. Shakouri, and A. C. Gossard, Phys. Rev. B **74**, 205335 (2006).
[20] G. Zeng, J.-H. Bahk, J. E. Bowers, J. M. O. Zide, A. C. Gossard, Z. Bian, R. Singh, A. Shakouri, W. Kim, S. L. Singer, and A. Majumdar, Appl. Phys. Lett. **91**, 263510 (2007).
[21] J. Zide, A. Kleiman-Shwarsctein, N. Strandwitz, J. Zimmerman, T. Steenblock-Smith, A. Gossard, A. Forman, A. Ivanovskaya, and G. Stucky, Appl. Phys. Lett. **88**, 162103 (2006).
[22] J. F. O'Hara, J. M. O. Zide, A. C. Gossard, A. J. Taylor, and R. D. Averitt, Appl. Phys. Lett. **88**, 251119 (2006).
[23] A. K. Azad, R. P. Prasankumar, D. Talbayev, A. J. Taylor, R. D. Averitt, J. M. O. Zide, H. Lu, A. C. Gossard, and J. F. O'Hara, Appl. Phys. Lett. **93**, 121108 (2008).
[24] L. V. Pourovskii, K. T. Delaney, C. G. Van de Walle, N. A. Spaldin, and A. Georges, Phys. Rev. Lett. **102**, 096401 (2009).
[25] K. T. Delaney, N. A. Spaldin, and C. G. Van de Walle, Phys. Rev. B **77**, 235117 (2008).
[26] X. Gonze *et al.*, Comput. Mater. Sci. **25**, 478 (2002).
[27] X. Gonze *et al.*, Z. Kristallogr. **220**, 558 (2005).
[28] The ABINIT code is a common project of the Université Catholique de Louvain, Corning Incorporated, and other contributors, http://www.abinit.org
[29] J. P. Perdew and Y. Wang, Phys. Rev. B **45**, 13244 (1992).
[30] D. M. Ceperley and B. J. Alder, Phys. Rev. Lett. **45**, 566 (1980).
[31] P. E. Blöchl, Phys. Rev. B **50**, 17953 (1994).
[32] N. A. W. Holzwarth, A. R. Tackett, and G. E. Matthews, Comput. Phys. Commun. **135**, 329 (2001).
[33] A. G. Petukhov, W. R. L. Lambrecht, and B. Segall, Phys. Rev. B **53**, 4324 (1996).
[34] H. J. Monkhorst and J. D. Pack, Phys. Rev. B **13**, 5188 (1976).
[35] M. Methfessel and A. T. Paxton, Phys. Rev. B **40**, 3616 (1989).
[36] J. S. Blakemore, J. Appl. Phys. **53**, R123 (1982).
[37] L. J. Sham and M. Schlüter, Phys. Rev. Lett. **51**, 1888 (1983).
[38] F. Giustino and A. Pasquarello, Surf. Sci. **586**, 183 (2005).
[39] A. Baldereschi, S. Baroni, and R. Resta, Phys. Rev. Lett. **61**, 734 (1988).
[40] M. Cardona and N. E. Christensen, Phys. Rev. B **35**, 6182 (1987).
[41] A. Baldereschi, Phys. Rev. B **7**, 5212 (1973).
[42] A. Schleife, F. Fuchs, C. Rodl, J. Furthmüller, and F. Bechstedt, Appl. Phys. Lett. **94**, 012104 (2009).
[43] J. R. Weber and C. G. Van de Walle (unpublished).
[44] W. A. Harrison, E. A. Kraut, J. R. Waldrop, and R. W. Grant, Phys. Rev. B **18**, 4402 (1978).
[45] K. Momma and F. Izumi, J. Appl. Crystallogr. **41**, 653 (2008).